Study the structural origin of the color effect of a colloidal gel in a binary solvent using USANS

2024 Neutron School on Small Angle Neutron Scattering and Neutron Reflectometry

NIST Center for Neutron Research
USANS Experiment
Yun Liu, Ryan Murphy, John Barker

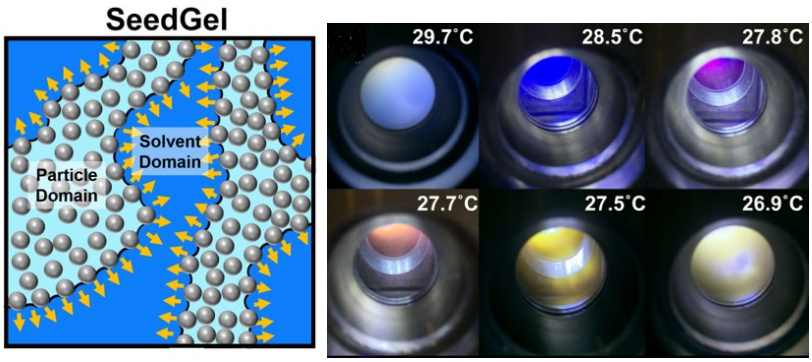

Abstract

The Ultra Small-Angle Neutron scattering (USANS) instrument at the NCNR is based on a Bonse-Hart design and can probe the structure with the length scale from about a few hundreds of nanometers to about twenty micrometers. It has been used to study a wide range of materials, such as shale, paints, and polymers. During this neutron school experiment, USANS will be used to study the structures of a new type of colloidal gels in binary solvents, the solvent segregation driven gel (SeedGel). When dispersing colloidal particles in a binary solvent, the microscopic phase separation of a binary solvent can lead to the formation of a SeedGel if the surface of particles is preferentially favored by one component of a binary solvent. In a SeedGel, the binary solvent becomes phase separated into two regions. Colloidal particles are all preferentially jammed in one solvent phase favored by particles to form a particle domain. The other component of the binary solvent forms the solvent domain. [1,2] SeedGel is thermo-reversible and scalable with very precise structure reproducibility during the temperature cycling. And some SeedGel systems show interesting dynamic coloration properties with temperature-controlled color change that can be finely adjusted over the entire visible spectrum [3] with interesting optical applications, such as smart windows and temperature sensors. Using the USANS instrument, we can investigate the domain size and understand how the temperature quenching rate determines the domain size. Various aspects of the experiment from the sample preparation and USANS instrument setup to data treatment and interpretation will be investigated, and references are given for more in-depth study. Even though the experiment focuses on the USANS instrument and their data analysis, we will also discuss how to analyze the SANS data of SeedGel to learn the local structural information of particles in the particle domain.

1. Introduction to colloidal particles in binary solvents

Colloidal systems consist of particles dispersed in a solvent with the size typically ranging from about one nanometer to about a couple of micrometers. The motions of particles are mostly driven by Brownian motions and the gravity effect typically does not play an important role for their mobility. These colloidal systems are commonly encountered in our everyday life, such as therapeutic drugs, paints, and shampoos.

The phase behavior of colloidal particle is determined by the effective interaction between these colloidal particles. If the interaction is dominatingly repulsive, particles tend to be away from each other so that they are stable in solutions even at fairly high particle concentrations. If the interaction is attractive, particles like to aggregate to form large clusters, cause the phase separation, or become a solid gel. This inter-particle interaction is influenced by both the direct interactions between particles, such as hard sphere interactions, and also the solvent molecules, such as counter ions, co-ions, and solvent fluctuations. The phase behavior of particles in a real system is equivalent to the phase behavior of colloidal particles interacting with this effective interaction potential. The effective interaction potential is considered as a coarse-graining method to simplify our way to investigate the structure and phase behavior of particles in a real system.

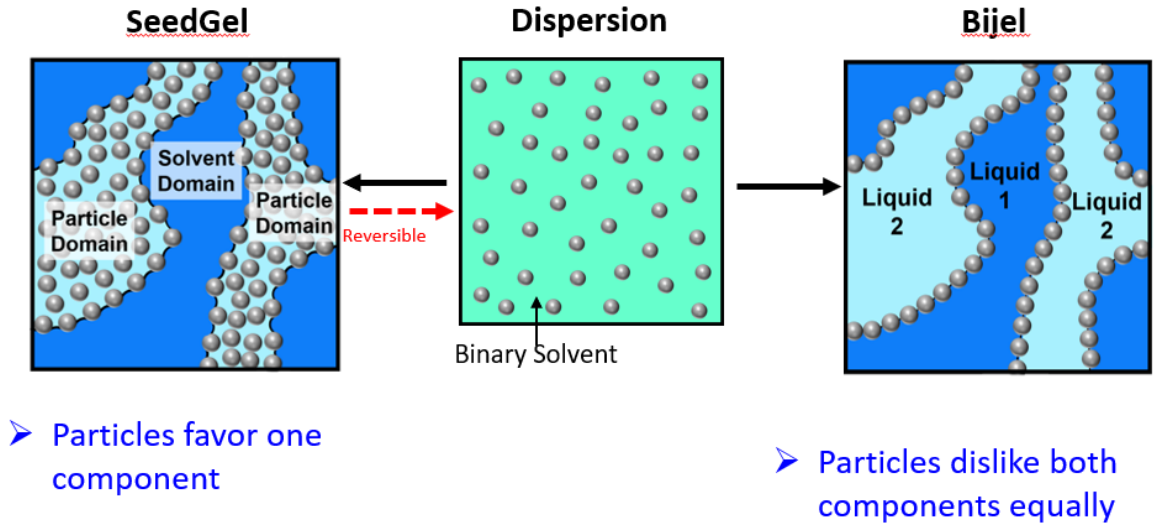

Figure 1. The schematic figures of SeedGel and Bijel to show the different structures of particles in a SeedGel and Bijel samples. Both types of gels are formed by dispersing particles in a binary solvent. Depending on the surface properties of a sample, a sample can become either a Bijel or a SeedGel by changing the sample temperature.

For particles dispersed in a binary solvent, the effective inter-particle interaction depends on the particle surface properties as well as the binary solvent. A binary solvent is made of two types of solvent molecules A and B that are partially miscible with each other. In 1978, Fisher and de Gennes showed that when the binary solvent condition moves closer to its critical point, there is an effective attraction generated between particles due to the long range solvent fluctuation.[4] This critical phenomenon induced attraction was also called critical Casmir forces,[5] and was found to be responsible for the aggregation behavior of silica particles dissolved in a binary solvent.[6] And when the attraction strength is strong enough, the particles can form a gel.[1,2] By tuning the surface of particles strongly favored by one component of the binary

solvent, it has been recently demonstrated that a system can form a SeedGel as shown in Figure 1.[1] Note that if the surfaces of particles dislike both components of the binary solvent, it can form a Bijel as also illustrated in Figure 1.[7,8] For the SeedGel, there is the phase separation of particles as well as the solvent. The solvent becomes two phase regions. Since particles like one component of the binary solvent, all particles are jammed into one solvent region to form particle domain. The other solvent region, consisting of mainly the solvent component the particles dislike, forms the solvent domain. Note that in a Bijel system, when the solvent phase separates, particles stay at the interface of the two solvent domains. One can consider that SeedGel and Bijel are two extreme cases for colloidal particles dissolved in a binary solvent. In this experiment, we plan to study the structures of a model SeedGel system: charged silica particles dissolved in a typical binary solvent, water/2,6-lutidine.

2. A model SeedGel system: charged silica particles in water/2,6-lutidine

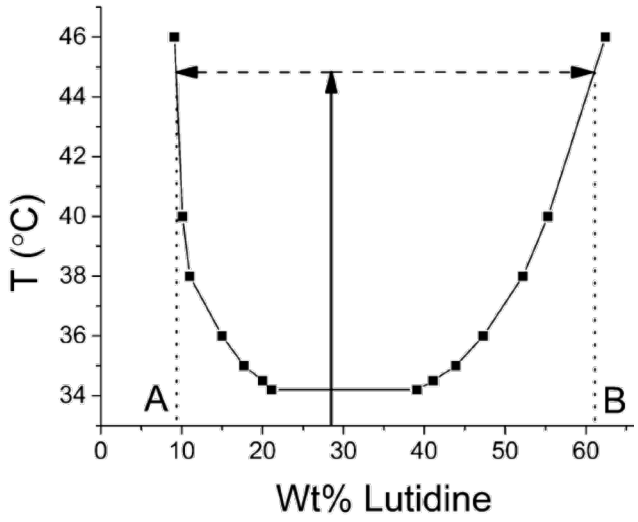

Figure 2. It shows the phase diagram of water/2,6-lutdidine. Water and 2,6-lutidine are miscible at low temperatures. However, when increasing the temperature above the demixing line (solid line), water and lutidine become phase separated. The critical temperature of this binary solvent is around 34 ºC. When charged silica particles are dissolved in water/2,6-lutidine at room temperature.

Figure 2 shows the phase behavior of the binary solvent with water and 2,6-lutidine, which is a lower critical solution temperature (LCST) system. The critical concentration for lutidine is about 29 % mass fraction with the critical temperature at about around 34 ºC for H_2O/lutidine.[9] Replacing H_2O with D_2O can decrease the critical temperature by a couple of degrees. At low temperature, water and 2,6-lutidine are fully miscible for any given relative concentrations of lutidine and water. When increasing the temperature, it becomes less soluble. Once crossing the demixing temperature, the bulk solvent becomes phase separated with two phases: one phase is rich in water and another phase is rich in lutidine. To prepare a sample to form a SeedGel, charged silica particles, whose diameter is about 27 nm, are added in the solvent with water/lutidine. Water in the binary solvent is preferentially adsorbed on the surface of the silica particles.[10] For the sample studied in this summer school experiment, the volume fractions for particles,

water, and lutidine in this sample are about 24 %, 53%, and 23% respectively. Because charged silica particles really like water, when heating the sample, it can form a SeedGel by increasing the temperature.

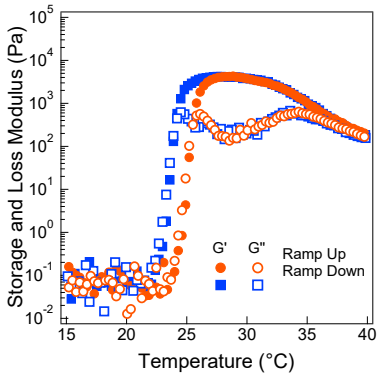

Figure 3. (a) Rheological behavior of the sample as a function of the temperature.

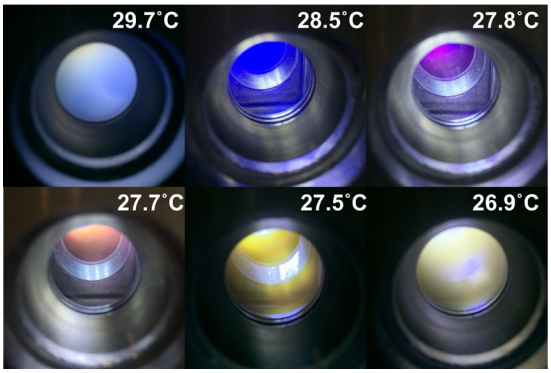

Figure 4. This SeedGel samaple shows different colors when there is a white light scoure behind the sample.

Figure 3 shows the storage (G') and loss (G") modulus of this sample at different temperatures. At room temperature, the sample remains as a tranparent liquid sample and both moduli are very small. However, when heating the sample, it becomes a solid gel at the temperatere from around 26 ºC to 34 ºC as G' becomes larger than G" within this temperature range. Later, we will show that the sample indeed becomes a SeedGel at this temperature range. And very interestingly, as shown by Figure 4, the sample shows different colors at differenent temperatures when putting a whilte light source behind of the sample. The color of the sample is reversibly adjustable by changing the sample temperature. All individual components of the sample (water, lutidine, and silica paritcles) do not show any color effect withint this temperature range. At low temperaature when the sample is liquid, the sample is transparent. Thus, the color effect of this SeedGel sample is driven by the structures formed in the SeedGel. It is thus very important to study the structures as a function of the tempearture and understand how to control the structures by the sample preparation.

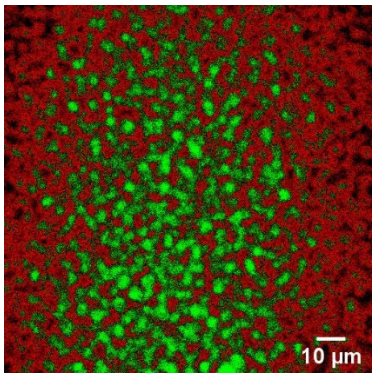

Figure 5. Confocal image of a SeedGel sample by adding dye molecules.

Preliminary confocal image of the SeedGel sample shows that the particles form a bicontinuous structures with the channel size at micrometer level. Therefore, we need a technique that can probe the structure at the length scale of a few micrometers.

Why use USANS?

Our experiment needs to probe the size information of the bicontinuous domains formed in the SeedGel. Because the domain size is at the micrometer level, its length scale is within the range of the length scales probed by USANS. Generally, static light scattering can access similar length scales. The contrast in light scattering arises from the difference in the refractive index between domains. At some temperatures, our samples become turbid as shown in Figure 3(b). Hence, there will be too much multiple scattering so that the light scattering is not a correct tool for those temperatures. USANS also overlaps in length scale with optical microscopy. However, since our samples are not transparent to light at some temperatures, it is difficult to study them with optical microscopes. But for the temperature ranges when the SeedGel sample is transparent, the samples can be studied also by the microscope and static light scattering. Ultra-small angle x-ray scattering (USAXS) does not generally reach as low q as USANS. In addition, x-rays (particularly at synchrotron sources) can damage samples. SANS/USANS is therefore an ideal probe for the structure of these systems. The combination of SANS and USANS allows the measurement of bulk samples over the whole relevant size range with no risk of sample damage.

3. The USANS Instrument

Fundamentally, a SANS/USANS experiment measures the number of neutrons scattered as a function of scattering angle. Since the size probed is inversely proportional to angle, to examine larger objects, we need to measure scattering at smaller angles. In the case of a "pinhole" SANS instrument this is achieved by changing the distance of a two-dimensional detector from the sample. The smaller angle a detector element subtends, the further the detector is from the sample.

The SANS instruments at the NCNR can measure the q value down to $8x10^{-4}Å^{-1}$ at their maximum sample to detector distance using lenses to focus the neutron beam. This implies a maximum size of measurable objects of approximately 500 nm. One can imagine simply making longer and longer instruments to study larger and larger objects. However, there are limitations to that approach. Firstly, neutrons have mass and

thus are affected by gravity. They fall on a parabolic path as they travel from the source to a detector. Secondly, the collimation requirements for longer instrument reduces the neutron flux onto the sample and increase the counting times. The count rate at the detector varies with the fourth power of the resolution. There is an alternative to a pinhole instrument using crystal diffraction before and after the sample in order to determine angular changes in the scattered beam. Such an instrument design is known as a Bonse-Hart type or Double-Crystal diffractometer (see Figure 6).

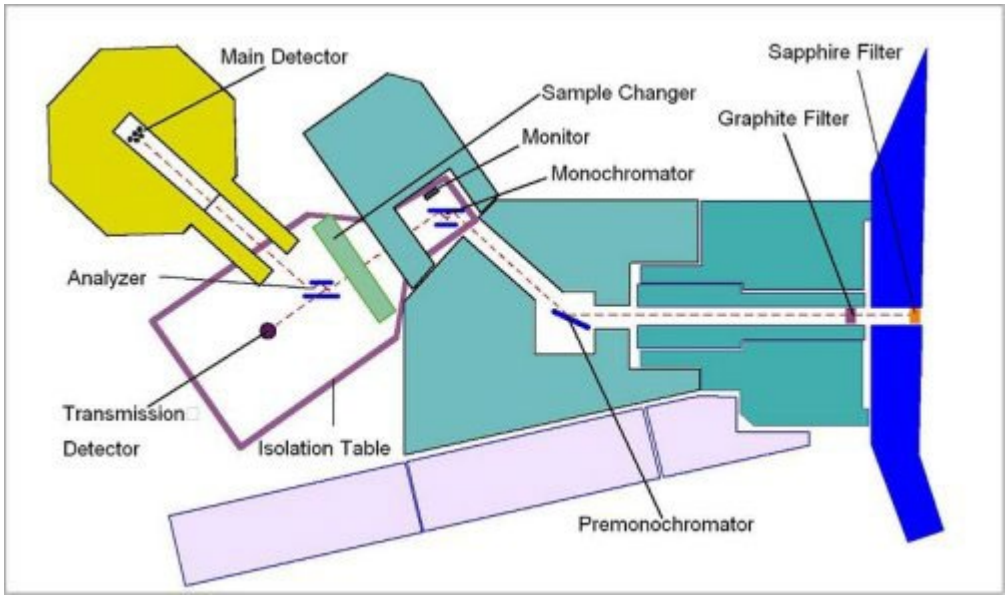

Figure 6: Schematic layout of the BT-5 USANS instrument. The dashed line indicates the beam path. The measured scattering angle, or momentum transfer q, is determined by rotation of the analyzer crystal.

Figure 6 shows the schematic layout of the NCNR USANS instrument which is located on beam tube 5 (BT-5). A channel cut silicon crystal (monochromator) directs the neutron beam onto the sample, where the neutrons are scattered. A second identical channel cut crystal (analyzer) is then placed in the scattered beam path and rotated to select the scattering angle to be analyzed and diffract the neutrons scattered at that angle into the detector. An experiment consists of rotating the analyzer to a series of angles and counting the number of neutrons that reach the detector. The intensity of scattering on the detector after background correction in a USANS experiment is given by

$$I_{cor}(q) = \varepsilon\, I_{beam} \Delta\Omega_A d_s T \left(\frac{d\sum_s(q)}{d\Omega}\right) \qquad (1)$$

where

ε is the detector efficiency

I_{beam} is the number of neutrons per second incident on the sample

d_s is the sample thickness

T is the sample transmission

$\Delta\Omega$ is the solid angle over which scattered neutrons are accepted by the analyzer

$\frac{d\sum_s(q)}{d\Omega}$ is the measured differential macroscopic scattering cross section, which is the true cross section modified by the instrumental resolution function.

The aim of a SANS/USANS experiment is to obtain the differential macroscopic scattering cross section $\frac{d\Sigma}{d\Omega}$ from I_{meas}. How we can go through that process is described later. But first we need to decide how to prepare our samples for the measurement.

4. Planning the Experiment

Given the stated objectives of the experiment and knowledge of the instrument, how do we prepare the experiment to maximize our chances of scientific success? Here we discuss some of the issues that are worth considering before an experiment.

4.1. Scattering Contrast

In order to have enough scattering intensity, there must be scattering contrast. The absolute intensity of the neutron scattering can be expressed as $I(Q) = \phi V \Delta\rho^2 P(Q) S(Q)$ for monodispersed spherical particles. Hence, the scattering is proportional to the scattering contrast, $\Delta\rho$, where

$$\Delta\rho = \rho_1 - \rho_2 \quad \leftarrow \text{Scattering Contrast} \tag{2}$$

and ρ_1 and ρ_2 are the scattering length densities (SLD) of the particles and the solvent, respectively. The scattering intensity is still proportional to $\Delta\rho^2$. And the contrast is the SLD of the two domains in the sample.

The SLD can be calculated using $\rho = \dfrac{\sum_{i=1}^{n} b_i}{V}$ (3)

where V is the volume containing *n* atoms, and b_i is the (bound coherent) **scattering length** of the i^{th} atom in the volume V. V is usually the molecular or molar volume for a homogenous phase in the system of interest.

The SLD of each component can be calculated from the above formula, using a table of the scattering lengths of elements. (The scattering length of different elements can be found at the NCNR website: https://www.ncnr.nist.gov/resources/n-lengths/.) It can be calculated using the interactive *SLD Calculator* at the NCNR's Web pages (http://www.ncnr.nist.gov/resources/index.html). In SANS experiments it is a common practice to deuterate one or more components to increase the contrast for the component under study. In particular, deuterating the solvent removes much of the incoherent background from the hydrogen, which is a limiting factor for many samples for measurements at high q (above 0.2 $Å^{-1}$), but this is not relevant for the USANS experiment.

Material	Chemical Formula	Mass Density (g/cc)	SLD (cm^{-2})
Water	H_2O	1.0	-0.56×10^{10}
Heavy water	D_2O	1.1	6.33×10^{10}
Silica particle	SiO_2	2.2	3.475×10^{10}
lutidine	C_7H_9N	0.925	1.156×10^{10}

Table 1. The scattering length densities (SLD) for the components used in this experiment.

Our sample has three components: H_2O, silica particles, and lutidine. The SLD of lutidine and H_2O is close to each other and the SLD of SiO_2 is much larger. The scattering data are expected dominated by the structures due to silica particles in the sample.

4.2. Sample Thickness

H**ow thick should one sample be?** Recall that the scattered intensity is proportional to the product of the sample thickness, d_s and the sample transmission, T. It can be shown that the transmission, which is the ratio of the transmitted beam intensity to the incident beam intensity, is given by

$$T = e^{-\Sigma_t d_d}, \quad (4)$$

where $\Sigma_t = \Sigma_c + \Sigma_i + \Sigma_a$, i.e. the sum of the coherent, incoherent and absorption macroscopic cross sections. The absorption cross section, Σ_a, can be accurately calculated from tabulated absorption cross sections of the elements (and isotopes) if the mass density and chemical compositions of the sample are known. The incoherent cross section, Σ_i, can be estimated from the cross-section tables for the elements as well. The coherent cross section, Σ_c, can only be estimated since it depends on the details of both the structure of the atoms in the sample. This should be no surprise as Σ_c as a function of angle is the quantity we are aiming to measure! The scattered intensity is proportional to d_sT and hence

$$I_{meas} \propto d_s e^{-\Sigma_t d_d} \quad (5)$$

which has a maximum at $d_s = 1/\Sigma_t$ which implies an optimum transmission, $T_{opt} = 1/e \approx 0.37$. The sample thickness at which this occurs is known as the "1/e-length". The NCNR web based SLD calculator provides estimates of Σ_i and Σ_a and gives an estimate of the 1/e-length as well as calculating the SLD.

4.3. Multiple Scattering

The analysis of small angle scattering data assumes that a neutron is scattered only once when passing through a sample so that the scattering intensity is simply related to the structure of the sample. However, if the scattering of a sample is very strong, multiple scattering may contribute significantly to the scattering signal. The analysis of a signal with strong multiple scattering is very challenging [6] and, sometimes, is essentially impossible. Thus when Σ_c is significantly larger than $\Sigma_i + \Sigma_a$ the thickness should be chosen such that the transmission due to the coherent scattering remains larger than 0.9, rather than 0.37 to avoid problems with the multiple scattering effect.

In this experiment, the sample thickness has been set to 1 mm.

4.4. Required q range

The q range that is routinely accessible using the BT-5 USANS instrument is $5x10^{-5}$ Å^{-1} to $5x10^{-3}$ Å^{-1}. Both low q and high q limits are in practice determined by whether there is measurable scattering above background since the analyzer can be set to count at any value of q. The high q value chosen for an experiment is usually determined by the length scales of relevance to a sample and whether overlap with the SANS measurement regime is required. Figure 7 shows the accessible q ranges of the SANS and USANS instruments. In this experiment we will be measuring to approximately $2x10^{-3}$ Å^{-1}.

5. Collecting data

As discussed earlier, the experiment consists of scanning the analyzer through a series of angles and counting the scattered intensity on the detector. The first step before collecting the scattering data, therefore, is to decide which angles to measure at and how long to count at each.

5.1. Configuring the instrument

We need to measure over a range of angles spanning two orders of magnitude in q and an appropriate q-spacing at low q-values would lead to a huge excess of data points at around q = $1x10^{-3}$ $Å^{-1}$.

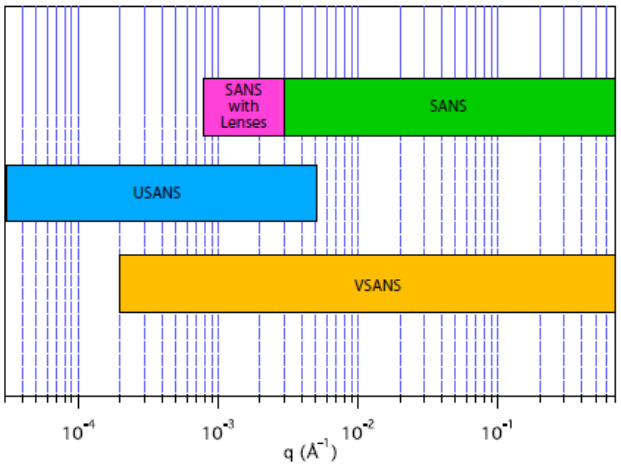

Figure 7: Comparison of the accessible q ranges of the BT-5 USANS instrument, NG-3 and NG-7 SANS instruments and the VSANS instrument currently under construction.

Usually, the scattering intensity is stronger at low Q values and varies greatly as a function of Q. We use closely spaced steps for Q at low Q and increase the step size gradually as the intensity variation decreases. Furthermore, we count for short times where scattering intensity is high, and gradually increase the counting times as the intensity diminishes. The scan spans the main beam and the peak intensity from that scan is used to determine the q = 0 angle, to scale the intensity into absolute units and to determine the sample transmission.

5.2. What measurements to make

To correct the instrument "background", a measurement of scattering without the sample is needed. Counts recorded on the detector can come from three sources: 1) neutrons scattered by the sample itself; 2) neutrons scattering from something other than the sample, but which pass through the sample; and 3) everything else, including neutrons that reach the detector without passing through the sample (stray neutrons or so-called room background) and electronic noise in the detector itself. In order to separate these contributions, we need to make three separate measurements:

1. Scattering measured with the sample in place (which contains contributions from all three sources listed above), $\boldsymbol{I_{sam}}$

2. Scattering measured with an empty sample holder in place (which contains contributions

from sources 2 and 3 above), $\boldsymbol{I_{emp}}$

3. Counts measured with a complete absorber at the sample position (which contains only the contribution from source 3 above), $\boldsymbol{I_{bgd}}$

The I_{bgd} on the USANS instrument is predominantly due to fast neutrons. This background is independent of instrument configuration as the fast neutrons are not coming along the beam path. It has been measured and is 0.018 s^{-1}, which equals 0.62 counts per 10^6 monitor counts. Thus, we do not usually measure a blocked beam run on USANS but use a fixed value for I_{bgd}.

5.3. How long to count

The uncertainty of the counting number due to the stochastic nature of the radiation (here, neutron) beam is important to understand the statistical error bar built into the scattering signal you collect. This uncertainty, or more precisely the standard deviation σ in the number of counts recorded in time, is given by $\sigma = \sqrt{N(t)}$. Here $N(t)$ is the total number of counts at certain detector position after counting for time t. Therefore, the relative error, $\sigma / N = 1/\sqrt{N} = 1/\sqrt{\gamma t}$, where γ is the average counting rate of a sample. Thus, increasing the counting time by a factor of four will reduce the relative error, σ / N by a factor of two. If there are 1000 total counts per data point, the standard deviation is $\sqrt{1000}$, which is approximately 30, giving a relative uncertainty of about 3%, which is good enough for most purposes.

A related question is how long the empty cell measurements should be counted relative to the sample measurement. The same $\sigma = \sqrt{N(t)}$ relationship leads to the following approximate relationship for optimal counting times

$$\frac{t_{bdg}}{t_{sam}} = \sqrt{\frac{CountRate_{bgd}}{CountRate_{sam}}} \qquad (6)$$

Hence if the scattering from the sample is weak, the background should be counted for as long as (but no longer than!) the sample scattering. If, however, the sample scattering count rate is, say, 4 times greater than the background rate, the background should be counted for only half as long as the sample. Since the scattering usually becomes much weaker at larger q, the time spent per data point increases with angle and the high q scans dominate the overall counting time.

5.4. Sample Transmission

The sample transmission is determined in two ways.

5.4.1. Wide angle transmission

A separate transmission detector (see figure 6), located behind the analyzer, collects all neutrons not meeting the Bragg condition for the analyzer. When the analyzer is rotated to a sufficiently wide angle from the main beam orientation this transmission detector counts both the direct beam intensity and the coherently small angle scattered intensity. Thus, the ratio of the count rate on the transmission detector with and without the sample is the sample transmission (T_{wide}) due to attenuation from incoherent scattering and absorption.

5.4.2. Rocking curve transmission

Rotating the analyzer through the main beam allows the intensity at q = 0 to be measured. The ratio of this intensity with and without the sample gives the transmission of the sample (T_{rock}) due to attenuation from incoherent scattering, absorption and coherent small angle scattering.

5.5. Multiple scattering estimate

The ratio of these separate transmission measurements can be used to estimate the amount of multiple scattering by

$$T_{SAS} = \frac{T_{Rock}}{T_{Wide}} = e^{-\tau} \quad (7)$$

If $T_{SAS} > 0.9$, the multiple scattering effect can be safely ignored. However, if $T_{SAS} < 0.9$, the multiple scattering becomes a concern.

5.6. Simulation of Scattering

Given enough information about the chemical composition of the sample and expected scattering properties, we can simulate the scattering to help us optimize the experimental setup. The reduction and analysis package provided by NCNR [6, 7] contains tools to help you do this.

The simulation takes input about your sample and simulates the data you would expect to collect on the instrument. This can guide you in deciding many of the factors discussed above such as appropriate sample thickness, counting time, and amount of multiple scattering. Additionally, it can help decide on the density of data points to be collected for USANS or the instrument configurations for SANS.

6. Data reduction

Data reduction consists of correcting the measured scattering from the sample for the sources of background discussed in section 4.2 and rescaling the observed, corrected data to an absolute scale of scattering cross section per unit volume. This is done via equation (5) presented previously and reproduced here for reference:

$$I_{cor}(q)_s = \varepsilon I_{beam} \Delta\Omega_A d_s T \left(\frac{d\sum_s(q)}{d\Omega}\right) \quad (8)$$

The beam intensity εI_{beam} is measured by rotating the analyzer through the direct beam at q = 0 with the empty cell in the beam path. The transmission T is measured by taking the ratio of the count rate observed on the transmission detector with and without the sample in the beam path. The solid angle of scattering accepted by the analyzer $\Delta\Omega_A$ is given by

$$\Delta\Omega_A = \left(\frac{\lambda}{2\pi}\right)^2 (2\Delta q_v)\Delta q_h \ , \quad (9)$$

where $2\Delta q_v$ is the total vertical divergence of the beam convoluted with the angular divergence accepted by the detector and Δq_h is the horizontal divergence accepted for the diffraction by monochromator and analyzer crystals. The instrument accepts scattered neutrons with $\pm\Delta q_v$=0.117Å^{-1}. The horizontal resolution Δq_h is measured from the full width at half maximum (fwhm) of the main beam profile obtained by rotating the analyzer through the direct beam. The fwhm when the crystal is properly aligned is 2.00 *arcsec*, equating to $\Delta q_h = 2.55\times10^{-5}$ Å^{-1} (the BT-5 instrument uses a mean wavelength λ=2.38Å), thus the solid angle over which neutrons are accepted by the analyzer is $\Delta\Omega_A$ = 8.6 x10^{-7} sr.

As you may have noted above, the analyzer has very good resolution in the horizontal direction and very poor resolution in the vertical direction as depicted graphically in figure 8. This is referred to as "slit geometry" as opposed to the "pinhole geometry" of a standard SANS instrument. The large difference between the horizontal and vertical resolutions means that the smearing can be treated as that from an "infinite" slit. The measured cross section, $d\Sigma_s / d\Omega(q)$ obtained from data reduction as described above is related to the true differential macroscopic cross section, $d\Sigma / d\Omega(q)$ by the relation [8]:

$$\frac{d\Sigma_s}{d\Omega(q)} = \frac{1}{\Delta q_v} \int_0^{\Delta q_v} \frac{d\Sigma}{d\Omega}(\sqrt{q^2 + u^2})du \qquad (10)$$

Figure 9 compares the scattering from a 1% volume fraction dispersion of 2 μm diameter silica particles with 5% polydispersity in D_2O using pinhole and slit geometries. Note the damping of the oscillations, the change in slope and reduction in intensity. Desmearing the data directly can be done by an iterative convergence method but the desmeared result is very unstable, being sensitive to noise in the data. The preferred method is to make use of equation (14) to smear a model function and fit the smeared data directly. The latter is the method we will employ in the analysis of our data.

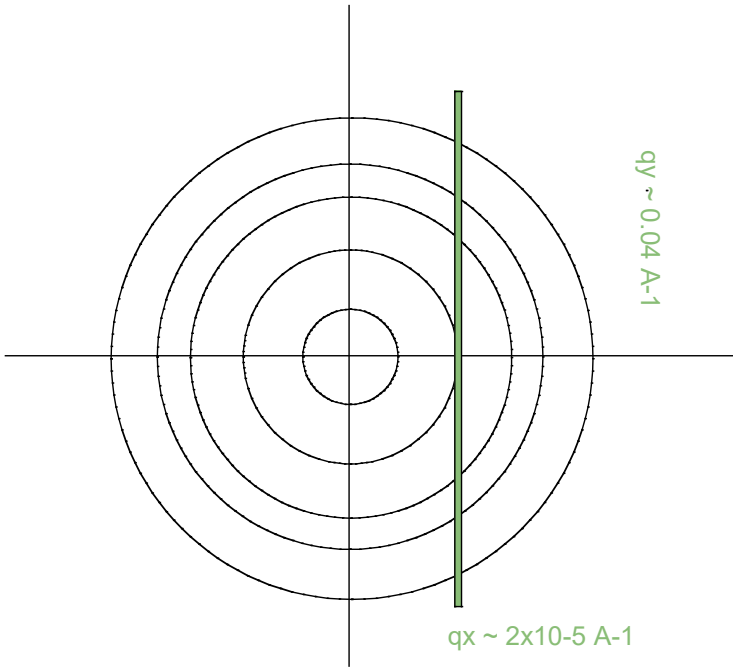

Figure 8: View of scattering with axes q_x and q_y collected by the analyzer on the BT-5 USANS instrument. The circles represent iso-intensity contours from isotropic small angle scattering. The narrow slit represents the scattering region collected by the analyzer.

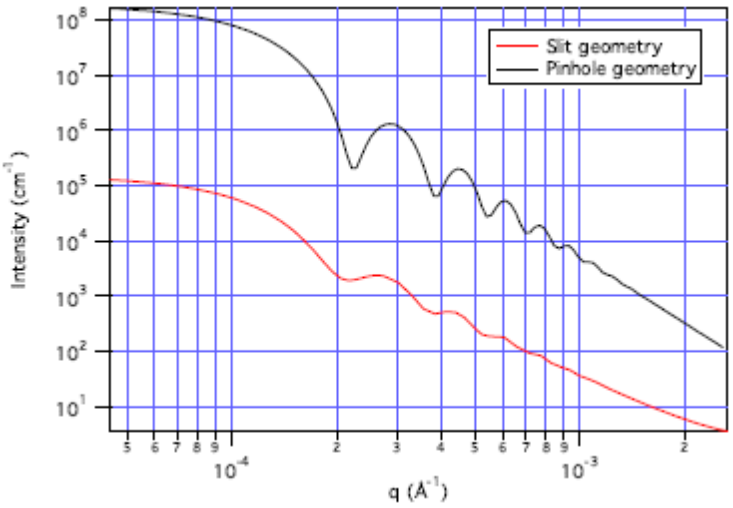

Figure 9: Comparison of the modeled scattering from a 1 % volume fraction dispersion of 2 μm diameter silica particles with5% polydispersity in D_2O using pinhole and slit geometries.

7. USANS Data Analysis

At the summer school we will use the IGOR USANS/SANS package to reduce the data and use SasView to analyze data collected from samples. The absolute scattering intensity I(q) for one sample is shown in Figure 10 (a). Below 26 ºC, the sample is in liquid state. There is no strong scattering feature in the Q range for the USANS except a relatively flat line. Once the sample is heated to 26 ºC, it becomes a SeedGel. And some large-scale structures are formed.

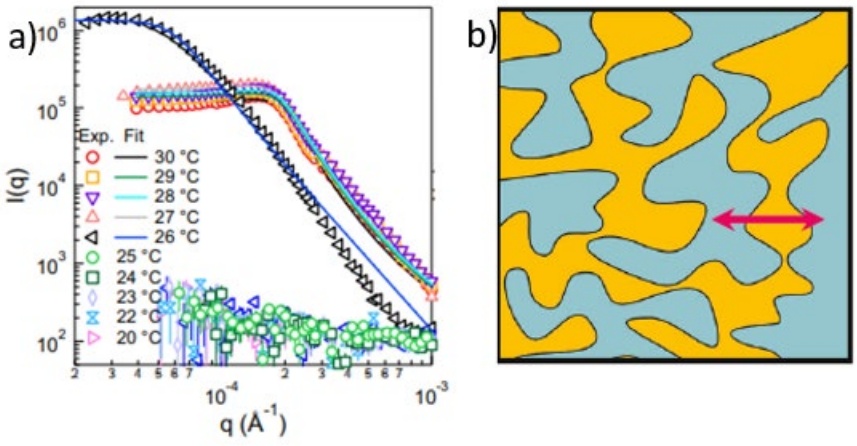

Figure 10. (a) USANS patterns of a sample in liquid states and gel states. (b) Schematic figure of two domains in the sample seen by USANS.

As shown in Figure 4, the formed structures are bicontinuous structures, which is also schematically shown in Figure 10(b). Since USANS only probe the structures at the large length scale (a few hundreds of nanometers and larger), the data for USANS are not sensitive to the detailed structures inside each individual domain. Thus, for USANS, the structures can be simplified to the schematical picture shown in Figure 10(b). The scattering is mainly due to the contrast between the particle domain and the solvent domain. It has been demonstrated that a scattering pattern with a bicontinuous structure can be fit with the Teubner-Strey model,[11] or T-S model, which can be expressed as

$$I(Q) = \frac{8\pi a_2 \langle \eta^2 \rangle / \xi}{a_0 + a_1 Q^2 + a_2 Q^4} \quad (11)$$

$$\langle \eta^2 \rangle = \phi(1-\phi)\Delta\rho^2 \quad (12)$$

$$d = 2\pi \left[\sqrt{\frac{1}{2}\sqrt{\frac{a_0}{a_2}} - \frac{1}{4}\frac{a_1}{a_2}} \right]^{-1} \quad (13)$$

$$\xi = \left[\sqrt{\frac{1}{2}\sqrt{\frac{a_0}{a_2}} + \frac{1}{4}\frac{a_1}{a_2}} \right]^{-1} \quad (14)$$

There are four fitting parameters for a T-S model, they are $\Delta\rho$, d, ξ, and ϕ. $\Delta\rho$ is the SLD difference between the particle domain and solvent domain. As the SLD of water and lutidine are similar, the difference of the two domains is mainly due to the existence of silica particles in the particle domain. ϕ is the volume fraction of one domain.

The T-S model can be better understood from the normalized Debye correlation function, $\gamma_0(r)$, which can be linked to the scattering pattern by the following equation

$$I(Q) = \langle \eta^2 \rangle \int \gamma_0(r) e^{i\vec{Q}\cdot\vec{r}} d\vec{r} \quad (15)$$

For a T-S model,

$$\gamma_0(r) = \frac{d}{2\pi r} \exp\left(-\frac{r}{\xi}\right) \sin\left(\frac{2\pi r}{d}\right) \quad (16)$$

From the Debye correlation function, $\gamma_0(r)$, the physical meaning of d and ξ becomes obvious. In the T-S model, it is assumed that the domains form a periodic structure with the average domain distance to be around d. Because there is no long-range order in the sample, the correlation length, ξ, is used to describe the loss of the long-range order in the sample. Note that the overall structures are still disordered. d should be considered as the average distance between different domains. Thus, the average domain size should be smaller than d. By fitting USANS patterns, we can extract the values of d so that we can investigate if there are structural changes of the bicontinuous domains during the temperature change when the sample color shows significant changes. Further, we will investigate what controls d during the sample preparation.

Interestingly, from 27 ºC to 30 ºC, there are little change of the USANS patterns even though there is a significant change of the color effect of the sample. Even without fitting the USANS patterns, it shows that the color change within this temperature range is not likely due to the large domain structural change of the SeedGel sample.

8. SANS data

The structure of a SeedGel sample is complex. Even though USANS experiments can probe the large length scale structure, i.e., the domain size information, they cannot provide the internal structure information of the particle domain due to the packing of nanoparticles with the diameter of about 27 nm. Because the particle size is small, SANS is used to probe the particle packings. The details of SANS instruments are covered by other experiments of the summer school. We only focus on the SANS data analysis of the SeedGel sample here.

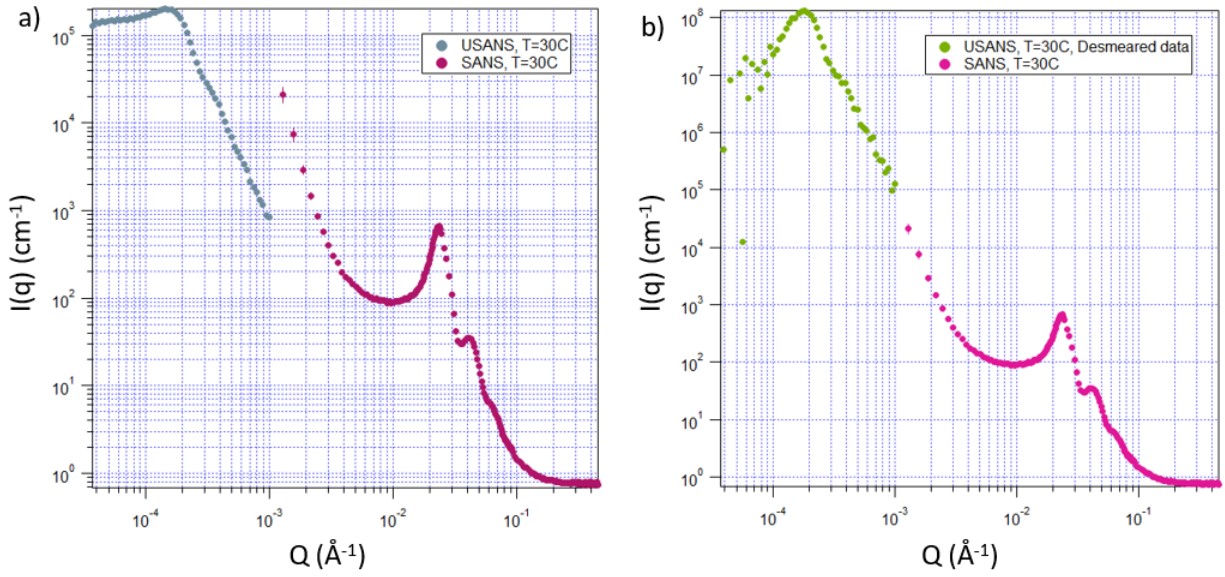

Figure 11. (a) USANS and SANS data for a SeedGel sample. (b) The desmeared USANS data are plotted together with the SANS data.

Figure 11(a) shows the USANS data and SANS data of a SeedGel sample in the same plot. The scattering intensity around Q=0.001 $Å^{-1}$ is dramatically different for USANS and SANS data. There is nothing wrong with the data or the measurement. This difference is actually expected due to the difference of the resolution function of the two instruments. As mentioned before, USANS has a slit smearing effect due to the instrument design. As a result, its intensity is the averaged intensity of the theoretical function in a wide Q range (mainly along the Q_y direction shown in Figure 8). Because the scattering intensity drops quickly when increasing the Q value, the averaged result is expected to be smaller. In comparison, the relative resolution of SANS has much smaller impact on the scattering intensity. Thus, the data from USANS and SANS are expected to be quite different at the same Q range. It is also known that due to the resolution smearing effect of the USANS, the power law decay is also affected by the slit smearing effect.

After desmearing the USANS data to remove the resolution function effect, the results in Figure 11(b) shows that the absolute intensity has a smooth continuation from the USANS Q range to the SANS Q range. Even though desmearing is useful to comparing the data from USANS and SANS, one needs to be aware that there are assumptions used during the desmearing process. To reliably extract the information from USANS data, one is encouraged to use a theoretical model to fit the data in Figure 11(a) by including the resolution function.

To prove particles are all packed in the water rich solvent phase, a contrast matching experiment was designed by mixing H_2O and D_2O so that the SLD of water matches to that of silica particles. If all particles are packed inside water rich solvent, the interaction peak at high Q (around 0.23 $Å^{-1}$) is expected to become very small. This is schematically illustrated in Figure 12(a). The SANS data in Figure 12(b) clearly indicate that the peak intensity at around 0.23 becomes very small. This experiment conclusively demonstrated that particles are indeed packed in the water rich phase region in the SeedGel. We will need to calculate the mixing ratio of H_2O and D_2O in order to match the water SLD with that of silica particles.

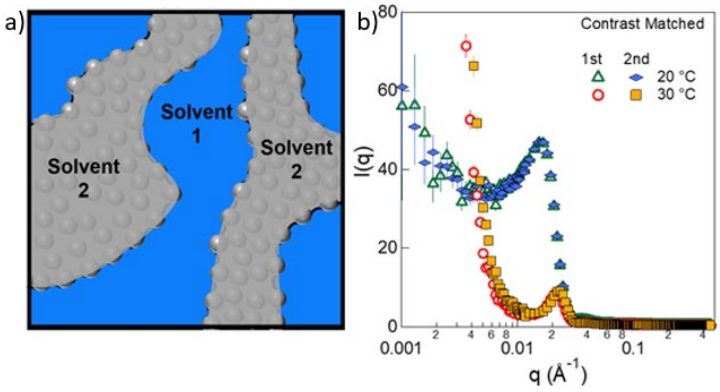

Figure 12. (a) Schematic picture to show that the SLD of solvent in water rich phase is matched to the SLD of silica particles. (b) the SANS data when the water SLD is matched to that of silica particles.

Figure 13 shows the SANS patterns of our sample at different temperatures. The sample was prepared using H_2O. At 20 ºC, the sample is in the liquid state and shows a broad peak that is typical for particles in liquid states. By increasing temperature to about 26 ºC , the sample becomes a SeedGel as shown by the rheological data in Figure 3. Note that when water SLD is not matched with silica particles, the peak at high Q becomes much stronger in Figure 13.

For the SANS data at $Q > 0.01$ $Å^{-1}$, the scattering patterns are mainly due to the particles packed inside the particle domain. Usually, the location of the main peak is correlated well with average distance between particles. Once becoming gel, the location of the main peak shifts to a larger Q value, which indicates that the inter-particle distance becomes smaller. This is consistent with the fact that all silica particles are packed inside the particle domain.

Interestingly, after the sample becomes a SeedGel, the scattering pattern does not change too much by further increasing temperatures. Thus, without any data analysis, it shows that the color change is not likely due to the change of particle packing structures inside the particle domain either.

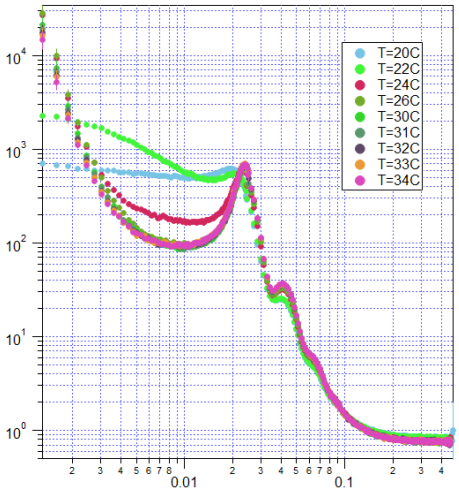

Figure 13 SANS patterns of the sample at liquid and gel states.

9. SANS data analysis

To fit the SANS data at high Q range, one needs to consider both the form factor, P(Q), and the inter-particle structure factor, S(Q), as the particle concentration is high in the particle domain. From the SANS fitting, we can extract the particle volume fraction in the particle domain.

In a liquid system at equilibrium conditions, the relative positions of colloidal particles are governed by the inter-particle potential. Any change of the potential affects the arrangement of colloidal particles in solutions and will be reflected by a corresponding change in the scattering pattern. For a monodisperse hard-sphere system the coherent scattering pattern $I(q)$ can be expressed as

$$I(q) = AP(q)S(q) \qquad (17)$$

where $A = \phi V \Delta\rho^2$, and ϕ, V, and $\Delta\rho$ are the volume fraction of the particles, the particle volume and the scattering length density contrast term respectively; $P(q)$ is the normalized form factor, which is only related with the shape of a particle, and $S(q)$ is the inter-particle structure factor that is related with the inter-particle potential. The scattering pattern of a dilute sample is thus determined by the form factor as $I(q) = AP(q)$. Once we have the information for $P(q)$ at small concentrations, we can extract $S(q)$ at higher concentrations.

$S(q)$ is essentially a measure of the correlation function of the relative positions of the center of mass of particles. If a system is at equilibrium, S(q) can be determined by the inter-particle potential and calculated using statistical mechanical theories. The details of how to calculate S(q) is beyond the scope of this simple lecture (see [12,13] for details). Because the particles are highly charged, we can model the interaction potential as a screened Coulombic potential. S(Q) for this kind of potential can be calculated to fit the experiment data. The theory originally proposed by Waisman in 1973 [14] was applied to study the charge interaction between colloidal particles by Hayter in 1983.[15] The Hayter_msa method is already implemented in SasView. We will use the SasView to fit the experiment data to obtain the approximate volume fraction of particles in the particle domain.

For a sample at liquid states, at relatively low concentration or high Q, $S(q) \approx 1$.

$$I(q) = \phi V \Delta\rho^2 P(q) \qquad (18)$$

Thus, the high Q data of concentrated solutions are dominated by the form factor. Interestingly, we can observe that there are slight changes of the intensity at high Q. Because the total volume fraction of silica particle is the same and the normalized form factor, P(Q), should remain the same, the only parameter that can affect the scattering pattern in Equation (18) at high Q is the contrast term, $\Delta\rho$, which is the SLD difference between silica particles and the solvent surrounding the particles. Because the SLD of silica particles is expected to be the same at the temperature range, the change of the contrast term can only be due to the change in the solvent SLD. Thus, changing the temperature in the SeedGel can cause the solvent composition change between the particle domains and the solvent domains. It is this solvent exchange between the two domains that introduces the color change of the sample when changing the same temperature.

Advanced discussion: Why is the solvent exchange responsible for the color change of a SeedGel sample?

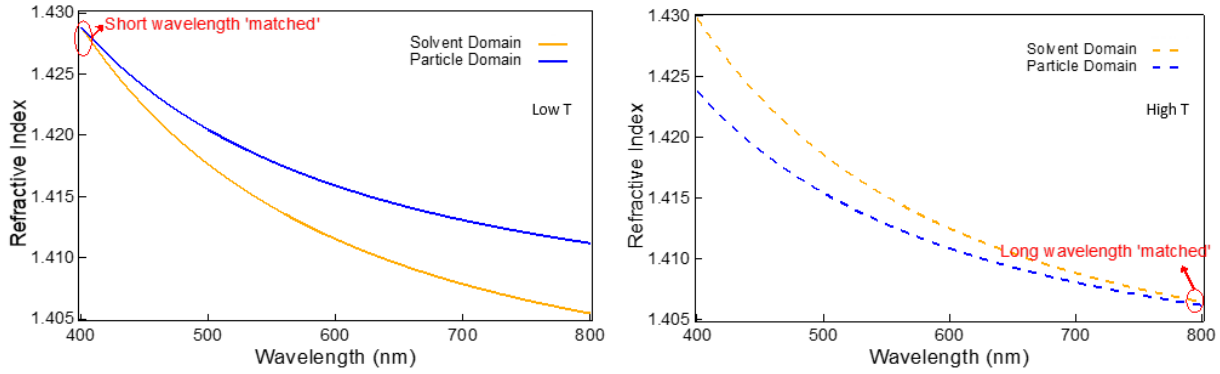

Figure 14. The calculated refractive index of the particle and solvent domains as a function of the wavelength.

The average refractive index of the two domains depends on the wavelength.[3] In Figure 14, the solid lines show the calculated refractive index of the particle domain (solid blue curve) and the solvent domain (solid orange curve) at low temperature for the SeedGel. It shows that the two lines match only at shorter wavelength. Thus, light with longer wavelength will be scattered away by the bicontinuous structures. Because red and yellow colors have longer wavelength, the structure color of a SeedGel sample shows a yellowish color at low temperature. However, when increasing the temperature, there is an exchange of solvent molecules between the two domains. The particle domain loses lutidine to the solvent domain and gains water from the solvent domain. Because the refractive index of water is smaller than that of lutidine, this solvent exchange decreases the average refractive index of particle domain and increases the average refractive index of the solvent domain. As a result, when increasing the temperature, the refractive index of the particle domains moves down in Figure 14 to become dashed blue curve while the refractive index of the solvent domain moves up from solid orange cure to dashed orange curve. Because of these shifts, the refractive index of the solvent and particle domain only matches at longer wavelength. Any light with longer wavelength will not be scattered and pass through the sample. The light with shorter wavelength are scattered at high temperature. Because light with shorter wavelength tends to be blueish, the SeedGel

sample shows blue color at high temperature. Because the solvent composition exchange is thermoreversible. The color change of a SeedGel is thus also thermoreversible. The physics mechanism of this phenomenon is called the Christiansen effect. The details are discussed in the Ref[3].

10. Summary

Through this experiment you shall learn the following concepts and understand how to apply them to gain useful information from your measurements:

Objectives of the Experiment:

- Get familiar with the USANS technique, how to optimize a sample for USANS and extract useful information from USANS scattering.
- Familiar with the Teubner-Strey model.
- Calculate the H_2O and D_2O ratio needed to match the water SLD with that of silica particles.
- Determine the form factor using a dilute sample.
- Familiar with the structure factor by fitting SANS data of concentrated samples.

Scattering theory

1) The Teuberner-Strey model for bicontinuous systems
2) Contrast matching experiment design.
3) What is the form factor, P(q)
4) What is the inter-particle structure factor, S(q)
5) The scattering contrast between colloidal particle and solvent
6) For a monodisperse system, $I(q) = AP(q)S(q)$
7) The colloidal interaction information can be extracted by fitting I(q)

Instrument information

1) The general principle of USANS
2) Transmission and scattering
3) Multiple scattering
4) Resolution functions
5) Counting statistics

References

[1]Y. Xi, R. S. Lankone, L.P. Sung, Y. Liu, Nature Communications, 12, 910 (2021).
[2]Y. Xi R. Murphy, Z. Zhang, A. Zemborian, S. Narayana, J. Chae, S. Choi, A. Fluerasu, L. Wiegart, Y. Liu, Soft Matter, 19, 233 (2023).
[3]Y. Xi, F. Zhang, Y. Ma, V. M. Prabhu, Y. Liu et al., Nature Communications, 13, 3619 (2022).
[4] M. E. Fisher and P.G. de Gennes, C. R. Acad. Sci. Paris B, 287, 207 (1978).
[5] T. W. Burkhardt, E. Eisenriegler, Phys. Rev. Lett. 74, 3189 (1995).
[6] D. Beysens and D. Estève, Phys. Rev. Lett., 54, 2123-2126 (1985).

[7] K. Stratford, R. Adhikari, I. Pagonabarraga, J. C. Desplat, M. E. Cates, Science, 309, 2198-2201(2005).
[8] E. M. Herzig, K. A. White, A. B. Schofield, W. C. K. Poon, P. S. Clegg, Nat. Mater. 6, 966-971(2007).
[9] Carlos A. Grattoni, Richard A. Dawe, C. Yen Seah, Jane D. Gray, J. Chem. Eng. Data, 38, 516-5129 (1993).
[10] C. E. Bertrand, P. D. Godfrin, Y. Liu, J. Chem. Phys. 143, 084704(2015).
[11] M. Teubner, R. Strey, J. Chem. Phys. 87, 3195-3200 (1987).
[12] Jean-Pierre Hansen and Ian R. McDonald, "Theory of Simple Liquids";
[13] C. Caccamo, "Integral Equation Theory Description of Phase Equilibria in Classical Fluids", Physics Report 274, 1-105(1996)
[14] E. Waisman, Mol. Phys. 25, 45 (1973)
[15] J. B. Hayter and J. Penfold, Mol. Phys. 46, 651 (1981).